

ACCUMULATION OF RESIDUAL DEFORMATIONS DUE TO CYCLIC LOADING WITH MULTIDIMENSIONAL STRAIN LOOPS

Mauro POBLETEⁱ⁾, Torsten WICHTMANNⁱⁱ⁾, Andrzej NIEMUNISⁱⁱⁱ⁾,
Theodor TRIANTAFYLLIDIS^{iv)}

ABSTRACT

A cyclic loading with multidimensional strain loops in the soil may be caused by traffic loading, by wind and wave loading (e.g. offshore wind turbines) or by earthquake shaking. The present paper focuses on the accumulation of permanent deformations due to a high-cyclic loading, that means a loading with many cycles of small to intermediate strain amplitudes. Two different strategies for the consideration of multidimensional strain loops in a high-cycle accumulation model are presented. Experimental evidence for the first strategy is provided. However, it is suitable for convex strain loops only. The second strategy can handle also non-convex strain loops, but has not been confirmed experimentally yet. The paper discusses suitable experiments for such prove and documents some preliminary test series.

Keywords: cyclic loading, multi-dimensional strain loops, permanent strain accumulation

INTRODUCTION

A cyclic loading may lead to an accumulation of permanent deformations in the soil. Inhomogeneities in the soil or a different loading of neighbored foundations may cause differential settlements, which may endanger the serviceability of a structure or even cause damage in statically indetermined structures.

In order to estimate the permanent deformations already during the design phase, Niemunis et al. [7] have developed a high-cycle accumulation (HCA) model. In finite element calculations the model is used along with a special calculation procedure which is shown schematically in Figure 1. Only a few cycles are calculated with a conventional (e.g. elastoplastic or hypoplastic) constitutive model formulated in terms of stress and strain rates. These parts of the calculation are necessary in order to estimate the field of the strain amplitude. During these cycles, for each integration point in the FE model, the strain loop is recorded as a series of discrete strain states. From the recorded strain loop the strain amplitude ε^{amp} is calculated which is an important input parameter for the HCA model. Different strategies for the calculation of

ⁱ⁾Research assistant, Institute of Soil Mechanics and Rock Mechanics, Karlsruhe Institute of Technology, Karlsruhe, Germany, e-mail: mauro.poblete@ibf.uka.de

ⁱⁱ⁾Research assistant, Institute of Soil Mechanics and Rock Mechanics, Karlsruhe Institute of Technology, Karlsruhe, Germany, e-mail: torsten.wichtmann@kit.edu

ⁱⁱⁱ⁾Research assistant, Institute of Soil Mechanics and Rock Mechanics, Karlsruhe Institute of Technology, Karlsruhe, Germany, e-mail: andrzej.niemunis@kit.edu

^{iv)}Professor and Director, Institute of Soil Mechanics and Rock Mechanics, Karlsruhe Institute of Technology, Karlsruhe, Germany, e-mail: theodoros.triantafyllidis@kit.edu

$\varepsilon^{\text{ampl}}$ for non-uniaxial strain loops are discussed in the following sections. Larger packages of cycles are calculated using a HCA model. The HCA model predicts the development of residual strain with the number of cycles without tracing the strain path during the individual cycles. The predicted accumulation rate depends on the strain amplitude, of the actual state of the soil (average void ratio, average stress) and of the cyclic preloading (number of cycles in the past) (Wichtmann et al. [13]). HCA models work similar to viscoplastic models with the number of cycles N replacing the time t . Therefore, the accumulation of deformations under cyclic loading is treated similar to the problem of creep under constant load. After a certain number of cycles it may be necessary to update the spatial field of the strain amplitude in a so-called "control cycle" (Figure 1) which is calculated conventionally again.

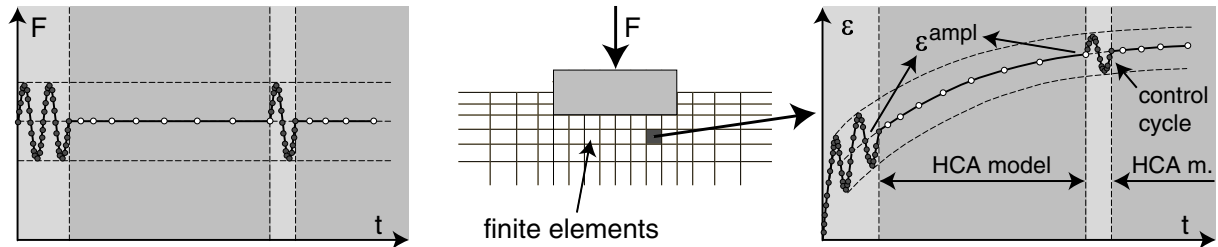


Fig. 1: Procedure for the FE calculation of the settlement of a shallow foundation under cyclic loading using a HCA model

For a number of practical problems the strain loops in the soil due to a cyclic loading are approximately one-dimensional, e.g. due to a repeated filling and emptying of tanks, silos and watergates or in the case of machine foundations. However, complicated multidimensional strain loops in the soil may result from earthquake shaking (Figure 2), from moving traffic loads (e.g. near railway tracks, Figure 3) and also in the case of offshore wind power plants, where the wind and wave loading may have different directions and frequencies.

The influence of the shape of the strain loop on the rate of strain accumulation and the handling of multi-dimensional strain loops in a HCA model is discussed in the following sections.

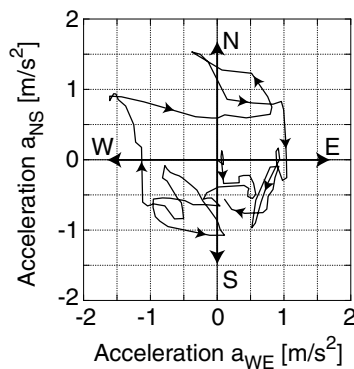


Fig. 2: Multidimensional acceleration loops due to an earthquake (Niigata, 1964, Ishihara [4])

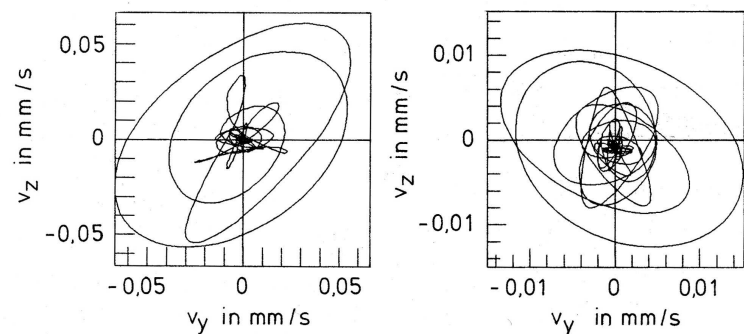


Fig. 3: Complicated velocity loops due to traffic loading, measurements of Huber [3]

LITERATURE REVIEW

A few experimental studies in the literature demonstrated a significant influence of the shape of the strain loop on the rate of residual strain accumulation or on the rate of pore water pressure accumulation, respectively.

Pyke et al. [9] subjected a dry sand layer to a multi-axial cyclic loading. Two shaking tables were mounted transversely on each other, allowing for 2-D shearing. If approximately circular shear stress cycles were applied, the settlements were twice larger than for uniaxial cycles with the same maximum shear stress (Figure 4). Furthermore, if two stochastically generated loadings $\tau_1(t)$ and $\tau_2(t)$ with $\tau_1^{\text{ampl}} \approx \tau_2^{\text{ampl}}$ were applied simultaneously, the resulting settlement was twice larger than in the case where the sand layer was sheared only with $\tau_1(t)$ or only with $\tau_2(t)$. If the shaking tables were additionally accelerated in the third, vertical direction, the accumulation rate was even larger. Pyke et al. [9] concluded that in the case of a multidimensional cyclic shearing in several orthogonal directions, the resulting settlement is identical with the sum of the settlements which would result from an uniaxial cyclic shearing in the individual directions.

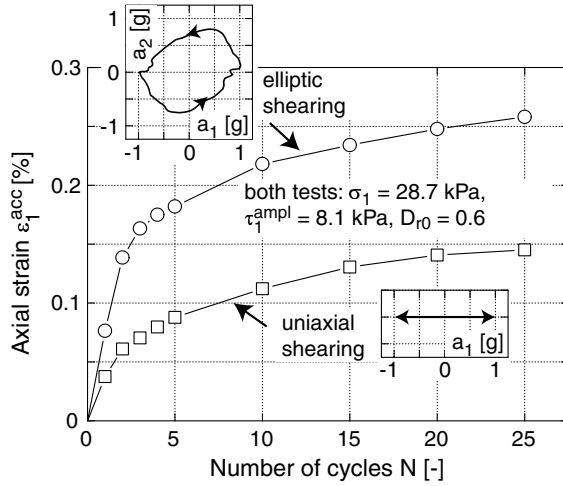


Fig. 4: Shaking table tests of Pyke et al. [9]: Comparison of uniaxial and circular stress cycles

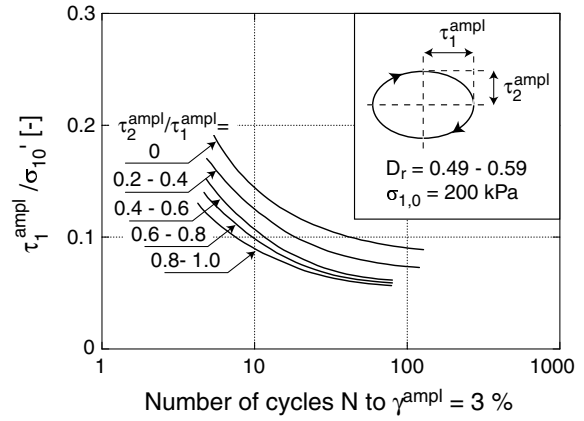


Fig. 5: Influence of the shape of the stress cycles on the liquefaction resistance after Ishihara and Yamazaki [5]

Ishihara and Yamazaki [5] performed undrained simple shear tests with a stress-controlled shearing in two mutually perpendicular directions. In a first series elliptic stress cycles were tested. The amplitude τ_1^{ampl} was kept constant and the amplitude in the orthogonal direction was varied in the range $0 \leq \tau_2^{\text{ampl}} \leq \tau_1^{\text{ampl}}$ (Figure 5). With increasing ratio $\tau_2^{\text{ampl}}/\tau_1^{\text{ampl}}$, the accumulation of excess pore water pressure was accelerated and the liquefaction (defined as the time at which a shear strain amplitude $\gamma^{\text{ampl}} = 3\%$ was reached) was achieved after a lower number of cycles (Figure 5). In a second series of tests, the specimens were sheared alternately in the τ_1 - and the τ_2 -direction (cross-shaped stress loops). A decrease of the liquefaction resistance was observed with an increasing ratio $\tau_2^{\text{ampl}}/\tau_1^{\text{ampl}}$.

The multidimensional simple shear tests performed by Wichtmann et al. [11] showed a twice larger accumulation rate for a circular cyclic shearing compared to one-dimensional cycles with the same maximum span (Figure 6). Niemunis et al. [8] performed cyclic triaxial tests with a simultaneous oscillation of the axial stress σ_1 and the lateral stress σ_3 in order to study the influence of the shape of the cycles. Different shapes of the cycles in the p - q -plane were tested, with $p = (\sigma_1 + 2\sigma_3)/3$ being the mean effective stress and $q = \sigma_1 - \sigma_3$ being the deviatoric stress. The resulting curves of the residual strain ε^{acc} versus the number of cycles N are given in Figure 7. Again the two-dimensional loops produce larger residual strains than the one-dimensional cycles. In the case of the one-dimensional cycles, a single change of the polarization by 90° undertaken at $N = 1,000$ lead to an increase of the accumulation rate. This effect was also observed in multidimensional simple shear tests (Wichtmann et al. [11]). Although the two-dimensional loops all had the same spans in the p - and in the q -direction, there are some subtle differences in the accumulation rates depending on the shape of the loops (compare circle,

diamond and cross in Figure 7).

It may be concluded that the influence of the shape of the strain loop on the rate of residual strain accumulation is quite significant. It has to be adequately considered in a HCA model.

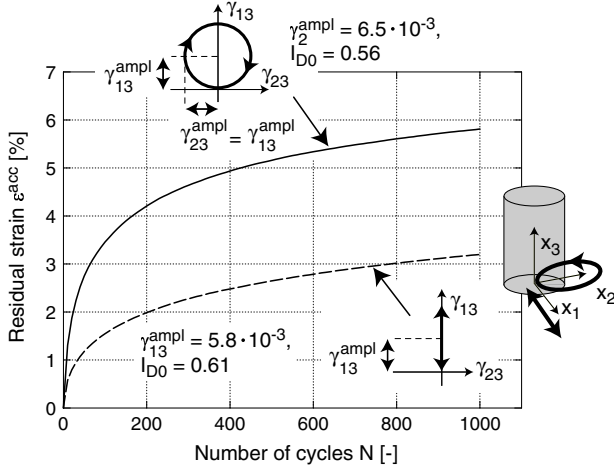


Fig. 6: Comparison of circular and one-dimensional strain loops in simple shear tests, Wichtmann et al. [11]

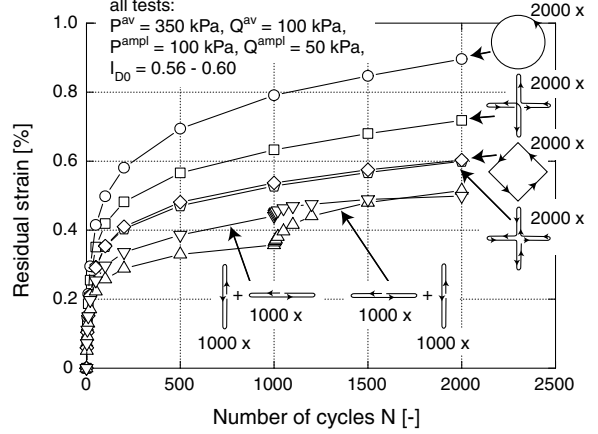


Fig. 7: Accumulation curves measured in triaxial tests with a simultaneous cyclic variation of σ_1 and σ_3 , Niemunis et al. [8]

AMPLITUDE DEFINITION FOR MULTIDIMENSIONAL CONVEX STRAIN LOOPS

The definition of a tensorial amplitude for multi-dimensional strain loops which is incorporated in the HCA model of Niemunis et al. [7] was originally proposed by Niemunis [6]. This definition is applicable to convex strain loops only. The procedure for the determination of $\varepsilon^{\text{ampl}}$ starts from the series of discrete strain points recorded during the conventionally calculated cycles (Figure 1). First, the span $2R^{(6)}$ (a scalar variable) of the in general six-dimensional strain loop is determined. The direction of the line connecting the two most distant points of the loop is denoted by $\bar{\mathbf{r}}^{(6)}$ (a second order tensor). After that the loop is projected into the direction $\bar{\mathbf{r}}^{(6)}$ onto a (hyper-) plane. The projected loop is five-dimensional. The span $2R^{(5)}$ and the direction of the projection are determined, and so on. The projections are illustrated in Figure 8, starting from a three-dimensional loop. Having finished the projections, six spans $2R^{(6)} \dots 2R^{(1)}$ and six directions $\bar{\mathbf{r}}^{(6)} \dots \bar{\mathbf{r}}^{(1)}$ are available. Then, the fourth-order amplitude tensor \mathbf{A}_ε is calculated as the sum of the dyadic products of the directions $\bar{\mathbf{r}}^{(i)} \times \bar{\mathbf{r}}^{(i)}$ weighted with the respective half span $R^{(i)}$:

$$\mathbf{A}_\varepsilon = \sum_{i=1}^6 R^{(i)} \bar{\mathbf{r}}^{(i)} \times \bar{\mathbf{r}}^{(i)} \quad (1)$$

The norm of the amplitude tensor is used as a scalar measure:

$$\varepsilon^{\text{ampl}} = \|\mathbf{A}_\varepsilon\| \quad (2)$$

In the special case of one-dimensional strain loops the scalar measure defined by Eqs. (1) and (2) is identical with the classical definition of the amplitude $\varepsilon^{\text{ampl}} = (\varepsilon^{\text{max}} - \varepsilon^{\text{min}})/2$. For two-dimensional elliptical cycles one obtains $\varepsilon^{\text{ampl}} = \sqrt{(R^{(1)})^2 + (R^{(2)})^2}$. Thus, circular loops with $R^{(1)} = R^{(2)} = R$ have an amplitude $\varepsilon^{\text{ampl}} = \sqrt{2}R$.

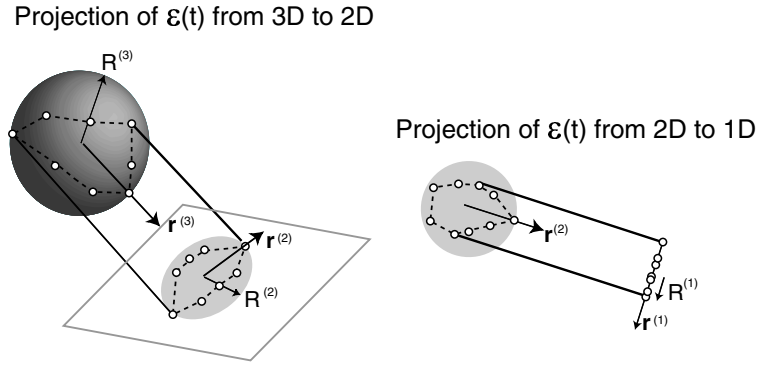


Fig. 8: Multiple projections of a strain loop in order to calculate an amplitude for multi-dimensional loops

The rate $\dot{\varepsilon}^{\text{acc}}$ of strain accumulation is approximately proportional to the square of the strain amplitude $(\varepsilon^{\text{ampl}})^2$ (Wichtmann [10]). This dependence has been implemented into the HCA model (Niemunis et al. [7]). Thus, for two-dimensional circular strain loops with a radius R (amplitude $\varepsilon^{\text{ampl}} = \sqrt{2R}$) the accumulation model predicts twice larger accumulation rates than for one-dimensional cycles with a span $2R$ (amplitude $\varepsilon^{\text{ampl}} = R$). The prediction of a twice larger accumulation rate for circular cycles is in good accordance with the test results shown in Figure 6. Thus, the amplitude definition for convex strain loops is experimentally confirmed for the two-dimensional case.

AMPLITUDE DEFINITION FOR MORE COMPLICATED STRAIN LOOPS

It has been recognized that the amplitude definition presented in the last section may not properly describe the accumulation rates due to more complicated strain loops as those shown in Figures 2 and 3 or those presented in Figure 9 (which have been generated by a superposition of harmonic functions). The definition of an amplitude and the counting of the cycles for such loops is not clarified yet.

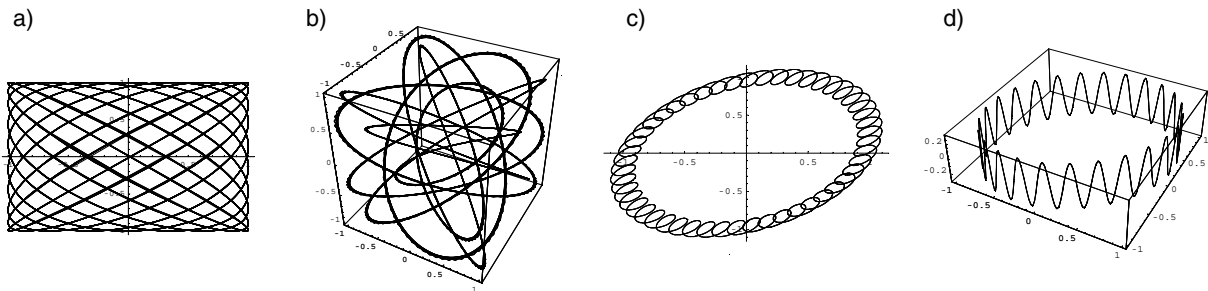


Fig. 9: Complicated strain loops, obtained by superposition of sine functions a), b) with slightly different frequencies and amplitudes or c), d) with strongly different frequencies and amplitudes

A possible treatment of such strain loops has been proposed by Niemunis et al. [8]. It is briefly summarized in the following. It has to be stressed that this procedure has not been verified experimentally yet.

The strain path $\varepsilon_{ij}(t)$ is assumed as a superposition of individual harmonic oscillations, which differ by their frequency f_K (or by their angular velocity $\omega_K = 2\pi f_K$, respectively). First, the single oscillations are extracted filtered from the entire signal. For each strain component $\varepsilon_{ij}(t)$ the portions belonging to a certain frequency f_K are extracted by means of a spectral analysis. Their sum constitutes a harmonic oscillation. In the general case it is a six-dimensional

ellipse in the strain space. The oscillations are numbered with the index K . The signal $\varepsilon_{ij}(t)$ is approximated as a sum of M oscillations:

$$\varepsilon_{ij}(t) \approx \sum_{K=1}^M \varepsilon_{ij}^{\text{ampl}K} \sin(\omega^K t + \varphi_{ij}^K) \quad (3)$$

For each strain component, the amplitude $\varepsilon_{ij}^{\text{ampl}K}$ and the phase shift φ_{ij}^K corresponding to the angular velocity ω^K are determined. Due to the over-proportional dependence of the accumulation rate on the strain amplitude, only the frequencies f_K with large amplitudes $\varepsilon_{ij}^{\text{ampl}K}$ have to be considered. For each oscillation the scalar measure

$$\varepsilon^{\text{ampl}K} = \|\varepsilon^{\text{ampl}K}\| \quad (4)$$

is determined with $\varepsilon^{\text{ampl}K}$ being a second order tensor collecting the amplitudes of the individual strain components ε_{ij} of the oscillation K . The same value $\varepsilon^{\text{ampl}K}$ would result from the procedure described in the last Section when it is applied to a strain loop where all strain components are described by harmonic functions with amplitudes $\varepsilon^{\text{ampl}K}$.

If M oscillations (i.e. M different frequencies) have to be considered the entire signal is decomposed into M packages of cycles each with an amplitude $\varepsilon^{\text{ampl}K}$ and a number of cycles N . It is assumed that these packages can be calculated in arbitrary sequence and that in this way the residual deformations can be estimated. Wichtmann et al. [12] have demonstrated that in the case of packages of one-dimensional cycles with different amplitudes, the sequence of application is of minor importance with respect to the final value of the permanent strain. However, a similar experimental study for multi-dimensional cycles is still missing.

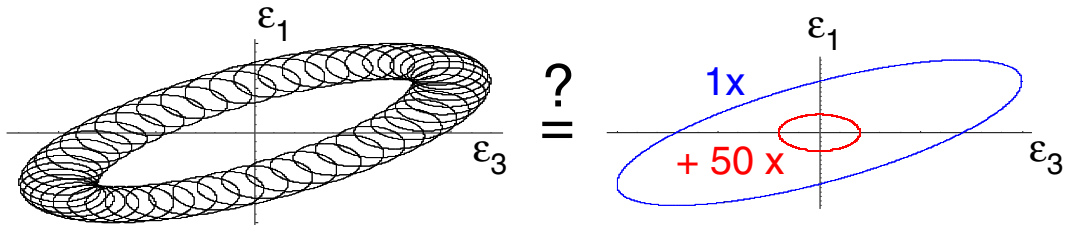


Fig. 10: Decomposition of a two-dimensional strain loop in two oscillations with different frequencies f_K

In order to prove the proposed procedure for the two-dimensional case, drained axisymmetric triaxial tests with a simultaneous oscillation of the axial and the lateral stress are planned. Strain loops obtained by a superposition of several harmonic functions with different frequencies and amplitudes will be tested (see the example in Figure 10). For comparison, in other tests on fresh samples, the same oscillations will be applied separately in succession. The sequence of application of the oscillations will also be varied. A decomposition of a strain loop into oscillations according to the procedure described above is justified if the tests with the complicated strain loops and those with the oscillations applied in succession deliver similar final residual strains.

In order to prevent an influence of membrane penetration effects on the data, the strains will be measured locally by means of local displacement transducers (LDTs) of the type described by Goto et al. [1] or Hoque et al. [2]. Specimens with a square cross section are advantageous for such measurements. Due to problems with the long-time stability of the LDTs under pressurized water, it is planned to perform the tests without water in the cell. The specimens will be tested in the dry condition, since otherwise the diffusion of air through the membrane into an initially water-saturated sample would influence the cumulative behavior. A fine sand ($d_{50} = 0.14$ mm, $C_u = d_{60}/d_{10} = 1.5$) will be used.

In preliminary test series it has been studied if the sample geometry influences the cumulative behavior, that means if cuboidal and cylindrical (standard) samples deliver the same results in long-term cyclic tests. Another preliminary study has been performed in order to clarify if dry and fully water-saturated specimens deliver the same results. The results of these test series are documented in the following sections. Furthermore, the calibration of the HCA model parameters for the fine sand is presented.

TEST RESULTS

Calibration of the HCA model parameters

First, the HCA model parameters C_{ampl} , C_e , C_p , C_Y , C_{N1} , C_{N2} and C_{N3} for the fine sand have been calibrated in stress-controlled drained cyclic triaxial tests with an uniaxial cyclic loading. The tests were performed on cylindrical samples with a diameter $d = 10$ cm and a height $h = 10$ cm. The specimens were prepared by pluviating dry sand out of a funnel into split moulds. After that they were flushed with CO_2 and saturated with de-aired water. A back pressure of 200 kPa was used in all tests. In each test 10^5 load cycles were applied with a frequency of 0.2 Hz.

17 tests with four different stress amplitudes q^{ampl} , seven different initial relative densities $I_{D0} = (e_{\text{max}} - e_0)/(e_{\text{max}} - e_{\text{min}})$, five different average mean pressures p^{av} and four different average stress ratios $\eta^{\text{av}} = q^{\text{av}}/p^{\text{av}}$ were performed. Figure 11 shows a typical plot of the vertical strain $\varepsilon_1(t)$ measured during the first 24 cycles and during five cycles recorded at $N = 50, 100, 200, \dots, 10^5$.

Figure 12a-d shows the increase of the residual strain ε^{acc} with increasing number of cycles N measured in the four test series. Evidently, the rate of strain accumulation increases with increasing amplitude (Figure 12a), decreasing density (Figure 12b) and increasing average stress ratio (Figure 12d). Similar residual strains were obtained in the tests with different average mean pressures because the tests were performed with the same amplitude-pressure ratio $\zeta = q^{\text{ampl}}/p^{\text{av}} = 0.3$ (Figure 12c).

The HCA model parameter C_{ampl} was determined from a curve-fitting of the function f_{ampl} (Table 1) to the data shown in Figure 12e. In that figure the residual strain ε^{acc} after different numbers of cycles is plotted versus a mean value of the strain amplitude, calculated as $\bar{\varepsilon}^{\text{ampl}} = 1/N \int \varepsilon^{\text{ampl}}(N)dN$. This averaging is necessary since the tests have been performed stress-controlled and thus the strain amplitude decreases slightly with N (especially during the first 100 cycles). On the ordinate the residual strain has been divided by the void ratio function \bar{f}_e of the HCA model (Table 1) in order to purify the data from the influence of slightly different initial densities and different compaction rates. \bar{f}_e has been calculated with a mean value of void ratio $\bar{e} = 1/N \int e(N)dN$. The parameter C_{ampl} given in Table 1 is the average of the values determined for different numbers of cycles.

A curve-fitting of the function f_e to the data in Figure 12f delivered the parameter C_e given in Table 1. In Figure 12f the residual strain has been divided by the amplitude function \bar{f}_{ampl} in order to purify the data from the influence of slightly different strain amplitudes. The data are plotted versus a mean value of void ratio. Since \bar{f}_{ampl} is necessary to purify the data in Figure 12f and \bar{f}_e is used on the ordinate in Figure 12e, the determination of C_{ampl} and C_e has to be done by iteration.

The parameters C_p and C_Y (Table 1) were determined from a curve-fitting of the functions f_p and f_Y (Table 1) to the data in Figures 12g and 12h. In those diagrams the residual strain has been divided by the amplitude and void ratio functions and plotted versus p^{av} or \bar{Y}^{av} respectively, where \bar{Y}^{av} is a normalized stress ratio which is zero for isotropic stresses and 1 on the critical state line.

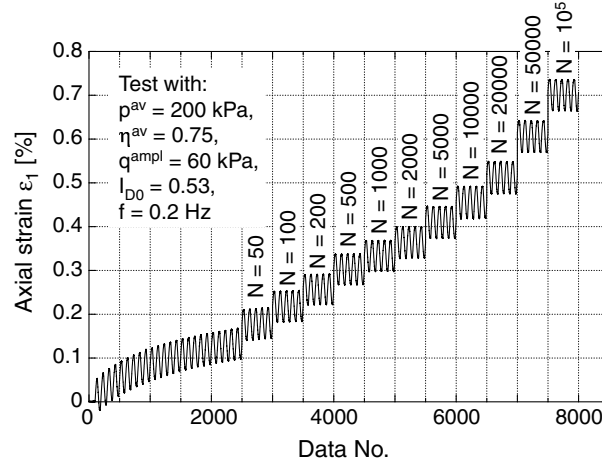


Fig. 11: Vertical strain $\varepsilon_1(t)$ measured during the initial phase of a drained cyclic triaxial test and after different numbers of cycles.

Function	Param.	Value
$f_{\text{ampl}} = (\varepsilon^{\text{ampl}}/10^{-4})^{C_{\text{ampl}}}$	C_{ampl}	1.31
$f_e = \frac{(C_e - e)^2}{1 + e} \frac{1 + e_{\text{max}}}{(C_e - e_{\text{max}})^2}$	C_e	0.58
$f_p = \exp[-C_p(p^{\text{av}}[\text{kPa}]/100 - 1)]$	C_p	0.22
$f_Y = \exp(C_Y Y^{\text{av}})$	C_Y	1.85
$\dot{f}_N^B = C_{N1} C_{N3}$	$C_{N1} [10^{-4}]$	2.82
$\dot{f}_N^A = C_{N1} C_{N2} \exp(-g^A/C_{N1}/f_{\text{ampl}})$	C_{N2}	0.37
$\dot{f}_N = \dot{f}_N^A + \dot{f}_N^B$	$C_{N3} [10^{-5}]$	2.64

Table 1: Functions of the HCA model and parameters for the fine sand.

The curves $\varepsilon^{\text{acc}}(N)$ from Figure 12a-d have been divided by the functions \bar{f}_{ampl} , \bar{f}_e , f_p and f_Y of the HCA model (Figure 12i) in order to determine the parameters C_{N1} , C_{N2} and C_{N3} . A curve-fitting of the function $f_N = C_{N1}[\ln(1 + C_{N2}N) + C_{N3}N]$ to the data in Figure 12i (solid curve) delivered the C_{Ni} -values specified in Table 1.

The slight differences between the set of parameters given in Table 1 and that determined by Wichtmann et al. [13] based on tests with isotropic average stresses needs further investigations. Probably the differences are due to deficits of the function f_Y of the HCA model.

The critical friction angle $\varphi_c = 33.1^\circ$ necessary for the cyclic flow rule \mathbf{m} of the HCA model has been determined from the inclination of a pluviated cone of dry sand. The calibration of the parameters for the elastic stiffness E of the HCA model has been discussed in detail by Wichtmann et al. [13].

Comparison of different sample geometries

Five drained cyclic triaxial tests with different sample geometries have been performed. Two cylindrical specimens were prepared with a diameter of 10 cm and a height of 10 cm (the standard size at our institute). Another cylindrical specimen was prepared with a diameter of 10 cm and a height of 20 cm (the size e.g. used by Wichtmann [10]). The two cuboidal specimens had dimensions $9 \times 9 \times 18$ cm. All samples were prepared by air pluviation and had a medium density ($0.54 \leq I_{D0} \leq 0.65$). They were tested in the water-saturated condition. The average

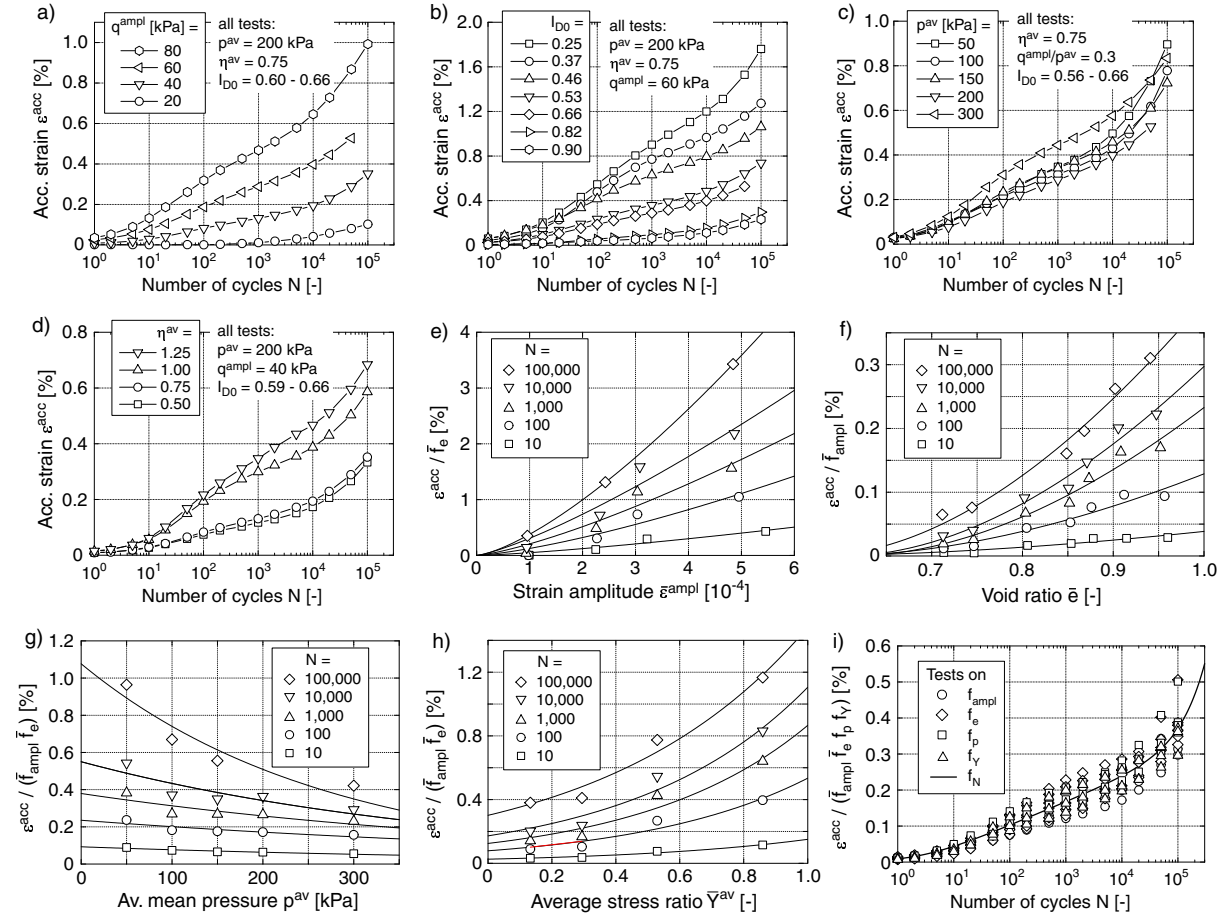


Fig. 12: Results of drained cyclic triaxial tests with different a,e) stress amplitudes q^{ampl} , b,f) initial relative densities I_{D0} , c,g) average mean pressures p^{av} and d,h) average stress ratios η^{av} . i) Determination of parameters C_{Ni} from a curve-fitting of the function f_N to the curves $\varepsilon^{\text{acc}}(N)/(\bar{f}_{\text{ampl}}\bar{f}_e f_p f_Y)$

effective stress ($p^{\text{av}} = 200$ kPa, $\eta^{\text{av}} = 0.75$) and the deviatoric stress amplitude ($q^{\text{ampl}} = 60$ kPa) were the same in all tests. All specimens were subjected to 10^5 cycles of axial load using a frequency of 0.2 Hz.

The same elastic and cumulative strains were measured for all sample geometries (Figure 13). The small differences in the accumulation curves (Figure 13a) and strain amplitudes (Figure 13b) are due to the slightly different initial densities. In Figure 13c the influence of density has been eliminated by dividing the accumulation curves by the void ratio function \bar{f}_e . The normalized accumulation curves $\varepsilon^{\text{acc}}(N)/\bar{f}_e$ for different sample geometries coincide well. Furthermore, no influence of the sample geometry on the "cyclic flow rule", that means on the ratio of the deviatoric and volumetric strain accumulation rates, could be detected.

Comparison of dry and water-saturated specimens

Seven drained cyclic triaxial tests on medium-dense specimens ($0.56 \leq I_{D0} \leq 0.61$) were performed. All specimens had a cylindrical shape ($d = h = 10$ cm) and were prepared by air pluviation.

One test was performed on a water-saturated specimen (the data of this test has been also included in Figure 12c). Five tests were performed on dry specimens. The constant lateral effective stress was applied via vacuum in two of these tests and via cell pressure in the three other ones. One of the tests with cell pressure was performed without a back pressure while a

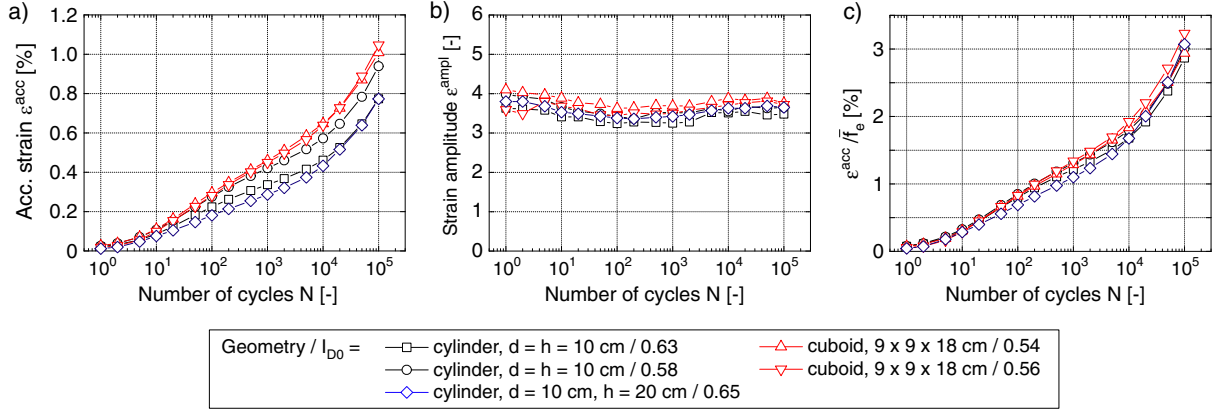


Fig. 13: Comparison of drained cyclic tests performed on specimens with different geometries.

back pressure of $u = 200$ kPa was applied in the two other tests. The purpose of the application of back pressure to the dry specimens was to achieve the same total stress level as in the test on the water-saturated specimen. A seventh specimen got moist due to a leakage of the membrane. At the end of that test a water content of 7.6 % was detected.

The average effective stress ($p^{av} = 50$ kPa, $\eta^{av} = 0.75$) and the deviatoric stress amplitude ($q^{ampl} = 15$ kPa) were the same in all tests. All specimens were subjected to an axial cyclic loading with a frequency of 0.2 Hz. The maximum number of cycles was chosen between 10^4 and 10^5 cycles.

Since volume changes could not be measured in the tests on the dry specimens, the data is given in terms of the axial strain ε_1 in Figure 14. The increase of the permanent axial strain ε_1^{acc} with increasing number of cycles is compared in Figure 14a. Obviously, the accumulation rates in the tests on dry sand were approximately twice lower than those measured in the test on the water-saturated specimen - independently whether the lateral stress was applied via vacuum or cell pressure and whether a back pressure is used or not. This observation can only partly be explained by the lower strain amplitudes measured for dry sand (Figure 14b). In order to eliminate the influence of the strain amplitude, the accumulation curves have been normalized by the amplitude function f_{ampl} in Figure 14c. However, the normalized accumulation curves of the dry specimens still plot below that of the fully water-saturated specimen.

These test results are somewhat surprising since in a similar test series performed on a medium coarse sand ($d_{50} = 0.55$ mm, $C_u = 1.8$) similar accumulation rates were measured for dry and water-saturated specimens at different loading frequencies (Figure 15). The lower elastic and cumulative strains for dry fine sand may be caused by electric charge of the grains.

The lowest accumulation rates were measured for the moist sample (Figure 14a). The strain amplitudes were similar to those of the dry specimens (Figure 14b). Therefore, the normalized accumulation curve for the moist sand in Figure 14c plots significantly lower than those of the dry and fully saturated specimens.

SUMMARY AND CONCLUSIONS

Experimental evidence for the significant influence of the shape of the strain loop on the rate of permanent strain accumulation due to a drained cyclic loading has been given. A definition of an amplitude for convex multi-dimensional strain loops has been experimentally confirmed for the two-dimensional case. This definition is incorporated into the high-cycle accumulation (HCA) model proposed by Niemunis et al. [7]. The applicability of a novel procedure for more

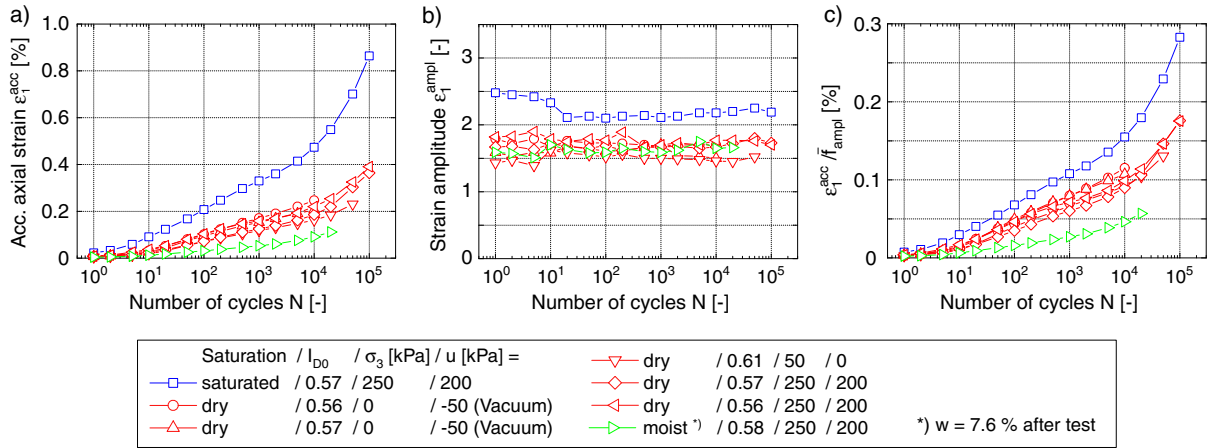


Fig. 14: Comparison of dry, moist and water-saturated specimens

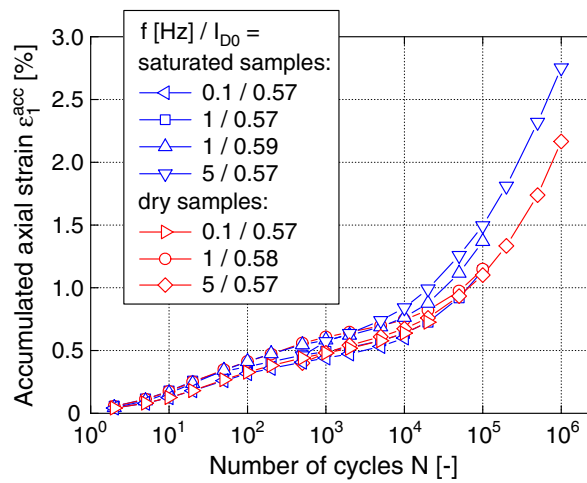


Fig. 15: Comparison of the accumulation curves measured in drained cyclic triaxial tests on a medium-coarse sand.

complicated strain loops has still to be checked experimentally. The procedure uses a decomposition of the strain path into several harmonic oscillations, which differ in their frequency. The idea is to filter these oscillations out of the entire signal and after that treat them separately. The results of some preliminary test series are presented in the paper. No influence of the sample geometry could be detected in drained cyclic triaxial tests on cylindrical samples with different heights and on cuboidal specimens. The accumulation rates and strain amplitudes of dry fine sand were found lower than those of water-saturated samples. Furthermore, the calibration of the HCA model parameters for the fine sand is shown.

ACKNOWLEDGEMENT

Parts of the research have been done within the framework of the project "Geotechnical robustness and self-healing of foundations of offshore wind power plants" funded by the German Federal Ministry for the Environment, Nature Conservation and Nuclear Safety (BMU, Project No. 0327618). Other parts were funded by DAAD and CONICYT in the framework of the PhD scholarship of the first author. The authors are grateful to BMU, DAAD and CONICYT for the financial support. The cyclic triaxial tests on the fine sand have been performed by the laboratory technician H. Borowski.

References

- [1] S. Goto, F. Tatsuoka, S. Shibuya, Y.-S. Kim, and T. Sato. A simple gauge for local small strain measurements in the laboratory. *Soils and Foundations*, 31(1):169–180, 1991.
- [2] E. Hoque, T. Sato, and F. Tatsuoka. Performance evaluation of LDTs for use in triaxial tests. *Geotechnical Testing Journal, ASTM*, 20(2):149–167, 1997.
- [3] G. Huber. Erschütterungsausbreitung beim Rad/Schiene-System. Promotion, Institut für Bodenmechanik und Felsmechanik der Universität Fridericiana in Karlsruhe, Heft Nr. 115, 1988.
- [4] K. Ishihara. Liquefaction and flow failure during earthquakes. The 33rd Rankine Lecture. *Géotechnique*, 43(3):351–415, 1993.
- [5] K. Ishihara and F Yamazaki. Cyclic simple shear tests on saturated sand in multi-directional loading. *Soils and Foundations*, 20(1):45–59, 1980.
- [6] A. Niemunis. Extended hypoplastic models for soils. Habilitation, Veröffentlichungen des Institutes für Grundbau und Bodenmechanik, Ruhr-Universität Bochum, Heft Nr. 34, 2003. available from www.pg.gda.pl/~aniem/an-liter.html.
- [7] A. Niemunis, T. Wichtmann, and T. Triantafyllidis. A high-cycle accumulation model for sand. *Computers and Geotechnics*, 32(4):245–263, 2005.
- [8] A. Niemunis, T. Wichtmann, and Th. Triantafyllidis. On the definition of the fatigue loading for sand. In *International Workshop on Constitutive Modelling - Development, Implementation, Evaluation, and Application, 12-13 January 2007, Hong Kong*, 2007.
- [9] R. Pyke, H.B. Seed, and C.K. Chan. Settlement of sands under multidirectional shaking. *Journal of the Geotechnical Engineering Division, ASCE*, 101(GT4):379–398, 1975.
- [10] T. Wichtmann. Explicit accumulation model for non-cohesive soils under cyclic loading. PhD thesis, Publications of the Institute of Soil Mechanics and Foundation Engineering, Ruhr-University Bochum, Issue No. 38, available from www.rz.uni-karlsruhe.de/~gn97/, 2005.
- [11] T. Wichtmann, A. Niemunis, and T. Triantafyllidis. On the influence of the polarization and the shape of the strain loop on strain accumulation in sand under high-cyclic loading. *Soil Dynamics and Earthquake Engineering*, 27(1):14–28, 2007.
- [12] T. Wichtmann, A. Niemunis, and T. Triantafyllidis. Strain accumulation in sand due to drained cyclic loading: on the effect of monotonic and cyclic preloading (Miner’s rule) (in print). *Soil Dynamics and Earthquake Engineering*, 30(8):736–745, 2010.
- [13] T. Wichtmann, B. Rojas, A. Niemunis, and Th. Triantafyllidis. Prediction of drained and undrained cyclic behaviour of a fine sand using a high-cycle accumulation model. In *Fifth International Conference on Earthquake Geotechnical Engineering, Santiago, Chile*, 2011.